Charge and Interfacial Behavior of Short Side-Chain Heavily Glycosylated Porcine Stomach Mucin

Gleb E. Yakubov,*,† Aristeidis Papagiannopoulos,‡ Elodie Rat,† and Thomas A. Waigh‡

Unilever Corporate Research, Colworth Park, Sharnbrook, Beds MK44 1LQ, United Kingdom and Biological Physics, Department of Physics and Astronomy, University of Manchester, Manchester M60 1QD, United Kingdom

Received June 28, 2007; Revised Manuscript Received September 20, 2007

The current accepted model for high-molecular-weight gastric mucins of the MUC family is that they adopt a polydisperse coil conformation in bulk solutions. We develop this model using well-characterized highly purified porcine gastric mucin and examine the molecules' charge and interfacial adsorption. "Orthana" mucin has short side-chains, low levels of sialic acid residues, and includes minute amounts of cystine residues that can be responsible for the self-polymerization of mucin. Atomic force microscopy and transmission electron microscopy are used to examine the interfacial behavior of the mucin and clearly demonstrate the existence of discrete spherical subunits within the mucin molecules, with sizes in agreement with static light scattering, dynamic light scattering, and ζ potential measurements. Furthermore images indicate the combs are assembled with a beads on a string conformation; the daisy chain model. Zeta potential measurements establish the polyampholyte nature of the mucin molecules, which is used to explain their adsorption behavior on similarly charged surfaces.

1. Introduction

Mucins are glycoproteins that are found ubiquitously in animal organisms.[1–3] These mixed protein/carbohydrate molecules have bulk functional properties that give rise to well-optimized viscoelasticities in many biological fluids such as saliva[4,5] or the gelled structure of gastric mucosa linings.[2,3,6–10] Furthermore, at biological interfaces, they greatly facilitate boundary lubrication, reducing damage to soft motile tissues.[11–15]

There are a wide variety of examples where mucins demonstrate a dual role functioning in the bulk as well as at the interface. Tooth pellicle is a complex formation comprised of salivary mucins and proline-rich proteins;[13,16–18] oral, GI tract, and respiratory airways have mucosa linings whose behavior is closely related to cilia motility,[3] tear secretions contain ocular mucins,[19,20] and in synovial joints, the active component of the lubricating layer on cartilage surfaces is a mucin-like biopolymer lubricin.[15,21–23]

Lubrication is known to be associated with the ability to form a dense hydrated layer at the surfaces of practically any chemistry,[12,16,24–28] including hydroxyapatite,[29] metals, and semiconductors.[17,30] This unique ability to adsorb is associated with the block-copolymer structure of mucins[31,32] that comprise glycosylated hydrated comb-brushes, polyampholyte domains with both positively and negatively charged amino acids, interspersed with domains that are rich in hydrophobic amino acids.[2] When adsorbed, the hydrophilic glycosylated comb sections stretch out into aqueous media due to favorable interactions with water,[6,12,24,33–38] thereby adopting a brush-like architecture even if the whole mucin molecule is adsorbed flat (Figure 1). The interaction between such mucin layers is characterized by a repulsive net force that includes both entropic (depletion) and electrostatic parts. [Comb side-chains of mucins are often negatively charged due to the presence of sialic acid residues ($pK_a \approx 2$) [8] and/or sulfate groups ($pK_a \approx 1$)[39].];[9,12,15,24,30,34,40–45] both factors are known to be crucial in biolubrication.[14,14,46–49]

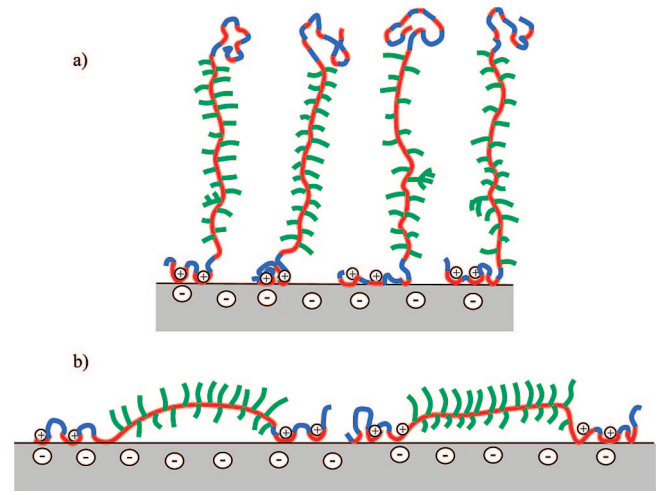

Figure 1. Conformation of adsorbed layers of mucins: (a) mucin brush; (b) flat conformation of adsorbed mucins with comb side chain forming a secondary brushlike layer. Green is the carbohydrate, red is positively charged protein, and blue is negatively charged protein.

The actual conformation of the adsorbed layers depends on the radius of gyration (R_g) of the mucin, the type of protein backbone, and the oligosaccharide sequence. Mucins and mucous glycoproteins can adopt either brush-like ($h > R_g$, where h is the layer thickness)[15] or flat architectures ($h < R_g$).[6,9,24,34,36,40,50–54] The flat layers are reported to correspond either to adsorbed coils,[55,56] extended threads (found primarily for ocular mucins[19,20,57–62]), or complex architectures.[50,53,63,64]

In the bulk, hydrophobic domains facilitate mucin self-association, and this aggregation mechanism stands alongside intramolecular disulphide bridging[2,3,5] or calcium-mediated

* Author to whom correspondence should be addressed. E-mail: gleb.yakubov@unilever.com.
† Unilever Corporate Research.
‡ Biological Physics, Department of Physics and Astronomy, University of Manchester.

10.1021/bm700721c CCC: $37.00
Published on Web 11/03/2007

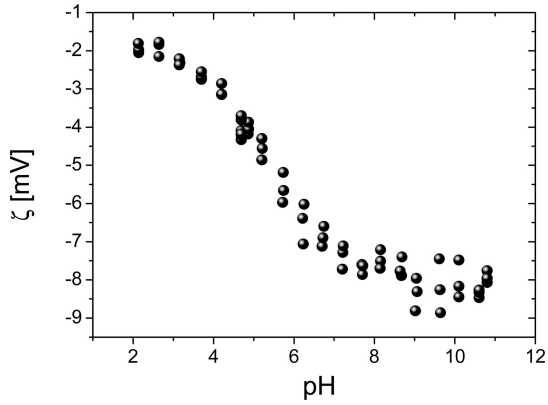

Figure 2. Dependence of the ζ potential of mucin on the pH of the solutions from electrophoresis experiments.

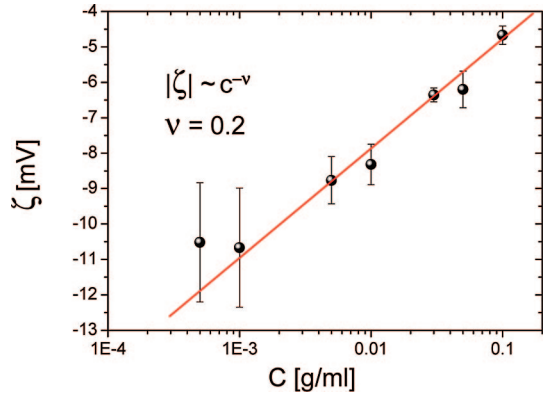

Figure 3. Dependence of the ζ potential on mucin concentration from electrophoresis experiments.

cross-linking[65] to promote the formation of strong viscoelastic gels. Association of mucin through hydrophobic domains has been confirmed by a number of reports,[2,8,10,39,51,52] but the surface architecture of such aggregates remains elusive.

In this report, we image the surface architecture of well-characterized mucins at hydrophilic substrates.[38] This tends to encourage the formation of globular surface adsorbed structures, as the hydrophobic domains on the mucins interact with each other more favorably than with the hydrophilic substrate. We have used highly purified short side-chain porcine gastric mucin similar to human MUC6 type, "Orthana" mucin. This mucin is characterized by short side chains, low levels of sialic acid residues, and includes minute amounts of the cysteine residues that are responsible for disulphide bridge formation. We find evidence for the daisy chain (dumbbell) configuration in the bulk that was suggested by us previously,[66] examine the charge and complex interfacial adsorption processes,[50,53,64] and demonstrate the formation of a two-dimensional network at lower pH values (pH < 4).[51]

2. Experimental Section

2.1. Mucin Preparation. Pharmaceutical grade porcine gastric "Orthana" mucin was purchased from A/S Orthana Kemisk Fabrik, Kastrup, Denmark. "Orthana" mucin is used in a saliva substitute formulation "Saliva Orthana" and originates from the linings of porcine stomachs. The commercial preparation was extensively dialyzed to remove all salts and other low-molecular-weight additives. It was lyophilized and stored for use as required. All solutions were made by dissolving weighed portions of the lyophilized material in ultrapure (resistance 18.2 M cm) water, the sample was shaken for 2 h, and

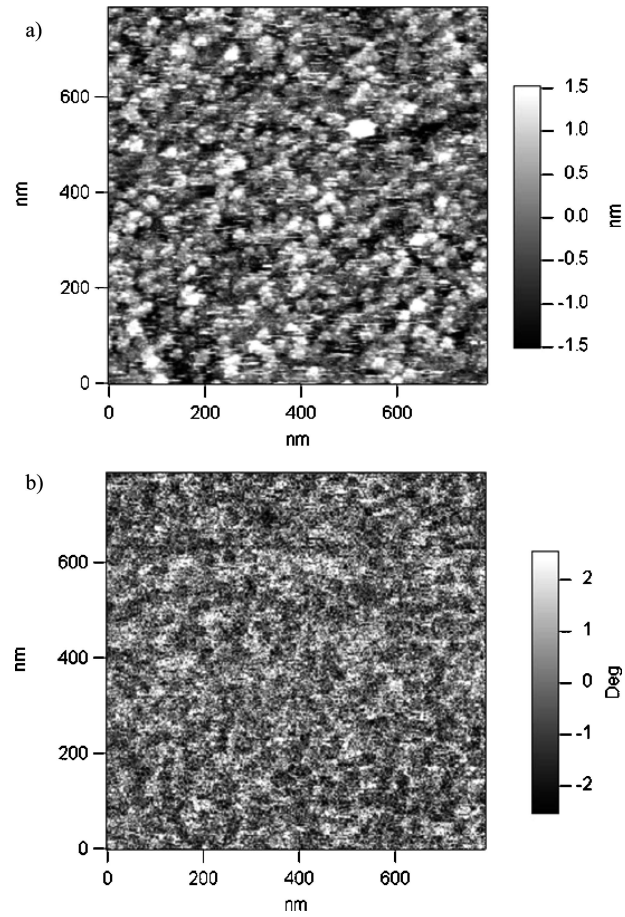

Figure 4. (a) AFM topography and (b) phase of mucin adsorbed film with a tapping force of 100 pN in the low bulk mucin concentration limit.

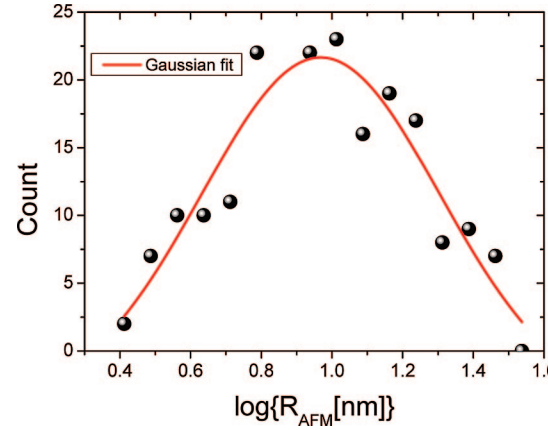

Figure 5. Size distribution histogram (R_{AFM}size in nm) for the globular features in the adsorbed mucin film at low bulk mucin concentrations.

subsequently filtered through a Sartorius "Minisart" filter (200nm pore size). The solutions were used immediately after preparation.

2.2. Electrophoresis. The measurements were performed using a ZetaSizer Nanoseries from Malvern Instruments. The measurements were conducted at 25 °C with disposable Folded Capillary Cells (Malvern, UK). The solutions had to be slowly injected through the cell to ensure that all the air bubbles were removed. All solutions were filtered through a Minisart sterile filter with a pore size of 0.2 μm.

The ζ potential was measured at several different values of pH, salt concentration (I_s), and mucin concentration. Seven mucin concentrations were examined in the range 1–100 mg/mL at constant salt concentration (10 mM NaCl). A constant mucin concentration (30 mg/ml) was

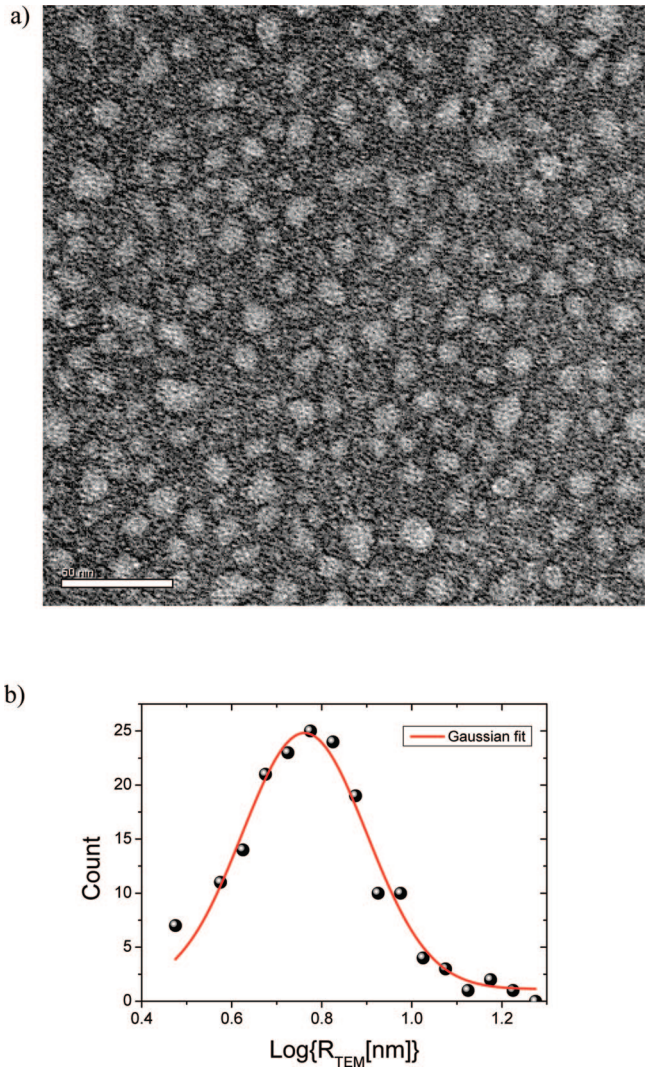

Figure 6. (a) TEM micrograph (bar 50nm) and (b) size distribution histogram of mucin film (2 mg/ml solution). A hydrophobic carbon film is used for the adsorption process.

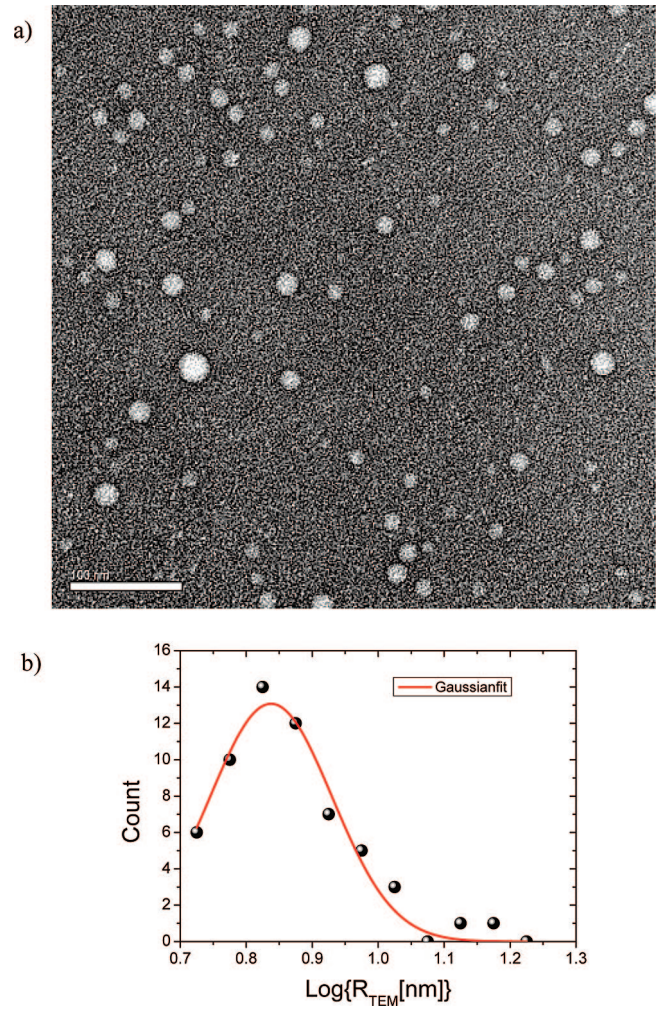

Figure 7. (a) TEM micrograph (bar 100nm) and (b) size distribution histogram of mucin films (1 mg/ml bulk solution). A hydrophilic carbon film is used for the adsorption process.

examined in different NaCl concentration solutions ranging from 1 mM to 1 M. Also a constant mucin concentration (30 mg/ml, 25 °C) was examined in different buffer solutions with pHs in the range 2–11. Furthermore, a constant mucin concentration (30 mg/ml) in 0.01 M NaCl solution was examined as a function of pH, titrated in a range 2 < pH < 11 using NaOH and HCl solutions with an autotitrator unit MPT-2 from Malvern Instruments.

2.3. Atomic Force Microscopy (AFM) Imaging. Atomic force microscopy images were obtained using a MFP-3D-IO instrument (Asylum Research, CA), an atomic force microscope integrated with an inverted optical microscope. For imaging, we used silicon tips (MikroMasch, Estonia, single beam shaped): (i) "CSC37/AL BS" for contact mode imaging, and AC mode in liquids, (ii) "NSC35/Al BS" for AC mode in air, and (iii) "NSC36/AL BS" for AC mode in liquids.

We used either a microscope slide glass or mica as a substrate for AFM imaging. All measurements were done at room temperature. Three methods of sample preparation were used:

Adsorbed Layers. a drop of mucin solution was deposited onto a glass/mica surface and incubated over a certain time (~20 min). Then the droplet was rinsed with the corresponding solvent. The substrate with an adsorbed film of mucin was either dried under a nitrogen jet for in-air images or instantly immersed in an aqueous solution (10 mM NaCl) for in-liquid imaging.

Arrested Layers. A drop of mucin solution was deposited on a glass/mica surface and incubated for 1–2 min Then the drop was dried under the nitrogen jet. This method allows for the arrest of nonadsorbed compounds present in the bulk solutions that are easily washed away by rinsing.

Dried/Rehydrated Layers. A drop of extremely dilute mucin solution was deposited onto a glass/mica surface and incubated in a nitrogen atmosphere in a laminar flow cabinet for a few hours until completely dry. All the material dissolved in the bulk solution accumulates on the surface that enables subsequent wet/dry imaging.

2.4. Transmission Electron Microscopy. TEM measurements were performed with a JEOL JEM-1200 EX II microscope. Mucin samples were prepared using deionized water, EtOH, and $NiCl_2$ solutions. The samples were negatively stained onto either a carbon-coated hydrophobic grid or a plasma-treated carbon-coated hydrophilic grid.

3. Results and Discussion

3.1. Electrophoretic Behavior of the "Orthana" Mucin. It was established from chemical analysis that "Orthana" mucin has predominantly neutral O-linked oligosaccharide side chains that provide essential hydrophilicity, allowing mucin to be dissolved relatively easily in water at concentrations of up to 200 mg/ml with no evidence of phase separation.[66] The presence of positively charged domains and hydrophobic amino acid residues suggests that mucin is a heterogeneous hydrophobic polyampholyte. The charge distribution was assessed using electrophoretic measurements, and it demonstrated good agree

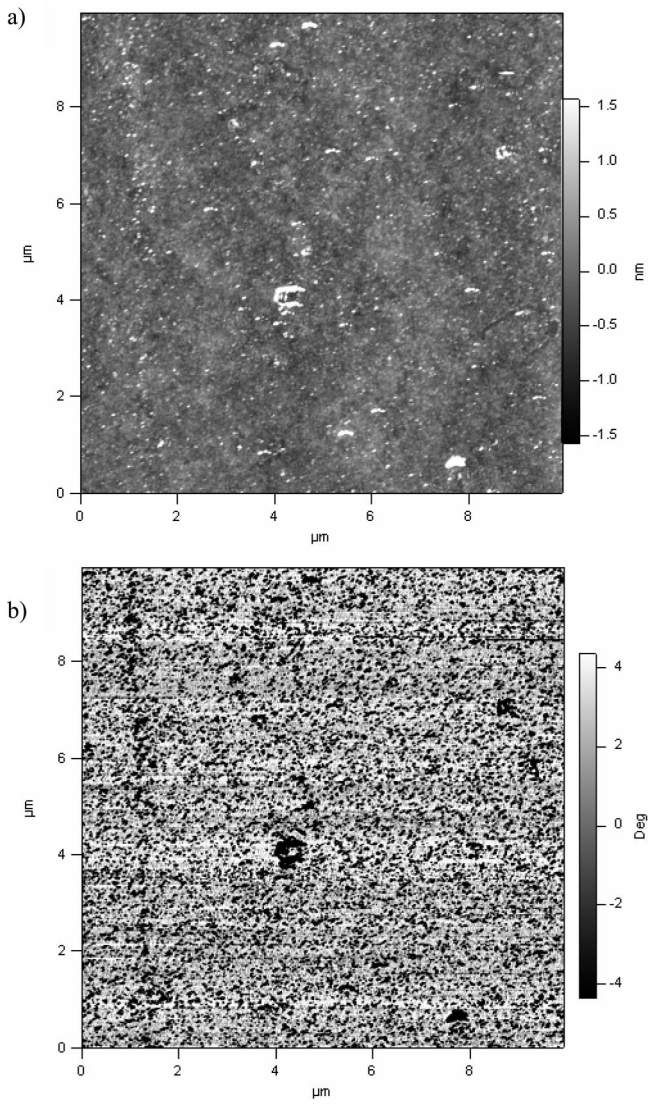

Figure 8. (a) AFM topography and (b) phase of dried mucin adsorbed film in the high bulk mucin concentration limit.

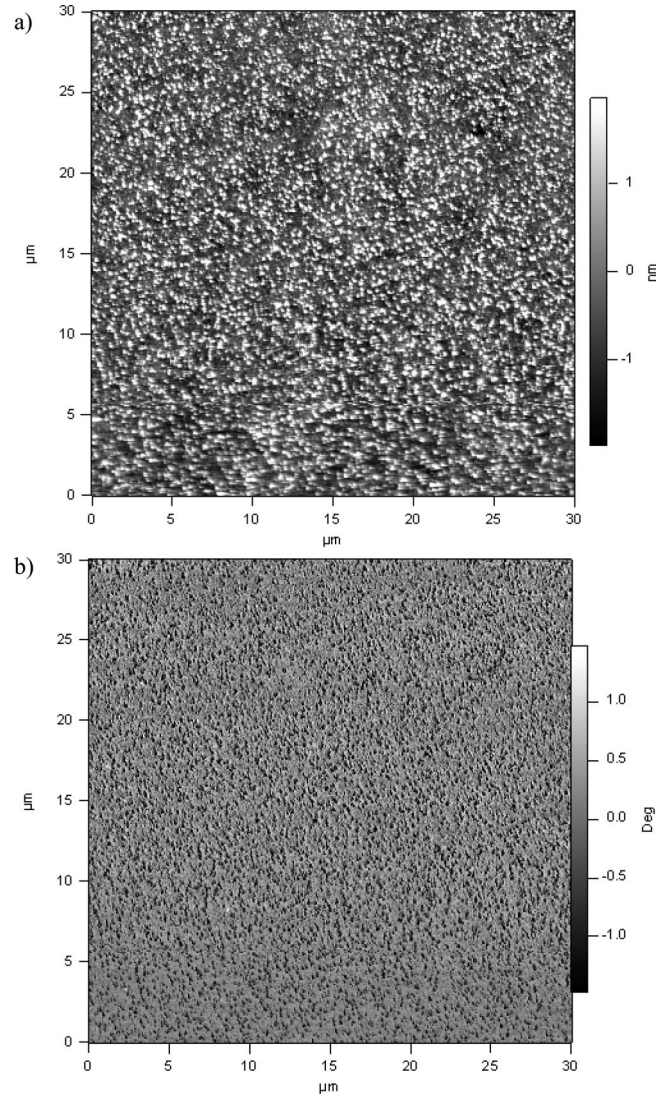

Figure 9. (a) AFM topography and (b) phase of mucin adsorbed film in 10 mM NaCl at the high bulk mucin concentration limit.

ment with the recent data of Spencer at al.[14] (Figure 2). The low values of the ζ potential and the asymptotic isoelectric point (the mucin molecule remains net negatively charged at all values of pH) suggest that mucin molecule is weakly charged. Mucin possesses both positively and negatively charged domains, so they must exist in a state of balanced charge regulation that prevents the mucin molecule from inverting its charge; the exact mechanism of such a charge regulation is unclear, but it may be realized through multiple mesoscale dipole moments within the mucin domains similar to those suggested by Dobrynin and Rubinstein for the necklace structure of polyampholytes in bulk solutions.[67]

The effect of mucin concentration in the low salt regime on the value of the ζ potential is presented in Figure 3. The scaling parameter is found to be equal to 0.2. The electrophoretic measurements are based on mobility detection via dynamic light scattering, and therefore the effective ζ potential corresponds to the charge at the hydrodynamic plane of shear. The apparent decrease in the absolute value of the ζ potential with increasing mucin concentration may be connected with structural changes within the bulk mucin solution due to the self-charge screening effect of neighboring charged molecules as they approach the semidilute overlap concentration. The ionic strength was found to have a small effect on the electrophoretic mobility of mucin up to relatively high salt levels of ~100 mM; above that level, we have observed an increase in mobility that we attribute to the shrinkage of mucin molecule as reported previously.[66] Here we can only hypothesize that the shrinkage leads to a consolidation of charges at the surface of the molecule that in turn lead to an increase in mobility.

For silica particles (r = 70 nm, BangsLabs, CA) modified with an adsorbed layer of "Orthana" mucin, we have observed an increase in the charge screening of the silica from −59.4±1 mV (bare silica particle, 10 mM background NaCl) to about −34.0±2 mV for mucin-coated silica particles, thus suggesting a partial electrostatic screening and a shift of the effective electrophoretic shear plane.

3.2. Structural Analysis of Adsorbed Layers. To find support for the daisy chain model for the mucin molecule,[66] we have performed AFM and TEM measurements on adsorbed and arrested layers. It is known that mucins can adsorb onto the surfaces of virtually any chemical nature. Mucin is a polyampholyte, and the adsorption phenomena on silicon oxide or mica can be explained within a framework of polyampholyte adsorption due to the polarization of chains by an external electric field created by the charged substrate.[67] According to this model, there are three basic configurations of the adsorbed

Table 1. Percentage of Coverage of Silicon Oxide Surface as a Function of Bulk Mucin Concentration from AFM Measurements

concentration of bulk mucin solution (mg/ml)	30.0	error (±)	1.0	error (±)	0.10	error (±)	0.010	error (±)
percentage coverage	14.8		13.1		11.6		6.4	
average area of the molecules (μm^2)	0.0357	0.0014	0.0268	0.0014	0.0176	0.0007	0.0120	0.0012
average radius of the surface adsorbed pancakes (R, nm)[72]	106.6	21.4	92.4	21.4	74.9	15.1	61.9	20.2

polyampholyte chain. (a) A pole regime observed when the electric field decay length is larger than the size of the chain. For mucins with a molecular weight of 546 kDa and radius of gyration 52 nm, this condition is not satisfied because the Gouy–Chapman length ($\lambda = 1/2\pi l_b \sigma \sim 10$ nm for a mica surface with ζ potential of -60 mV from conductivity measurements and the shear place is assumed to occur at 1nm from the surface) is always smaller than the chain size. For this type of structure, AFM visualization would be expected to detect a single "blob" that corresponds to the anchoring point[68] or an "empty/featureless" image that is due to the high flexibility of the polymer chain. The fence regime (b) occurs when the chain is confined within the Guy−Chapman length and is divided into subsections of size λ. These subsections are strongly attached to the surface and would be expected to be visualized in an AFM experiment. If λ is further decreased, then the system crosses over in to the pancake regime (c). In this case, all domains with charges opposite to that of the surface are within a distance λ of the surface. This conformation can be easily discriminated using AFM imaging because the density of a pancake is sufficient to generate a mechanical response on the cantilever.

As an initial step, a mucin layer was adsorbed from a very dilute solution (3×10^{-5} mg/ml) onto plasma-treated glass and the adsorption time was 30 min. By using low concentrations, the formation of multilayers was avoided that are typical in polyampholyte adsorption.[67] The softness of mucin molecules reduces the contrast of images due to contact deformation, and therefore great caution was taken in adjustments of the tapping force and the oscillation amplitude in order to minimize these distortions.

Figure 4 is a 800 nm field intermittent contact mode image taken using a tapping force of 100 pN. The height image depicts globular features that homogenously cover the surface. The complimentary phase image clearly depicts softer areas as darker spots.

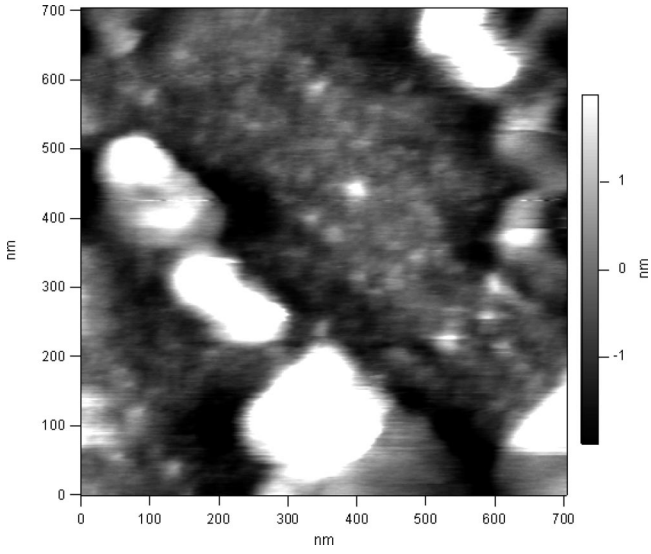

Figure 10. AFM topography of a complex adsorbed layer of mucin.

Figure 5 is a histogram of the distribution of lateral dimensions (R_{AFM}) based on the analysis of the AFM image (Figure 4). The value of R_{AFM} is found to be 9.5±3 nm. This value coincides with the dimensions of the internal daisy beads of a mucin molecule determined previously using dynamic light scattering;[66] the observed results also agree with the recent work of Hong at al.[51]

To acquire complimentary data, transmission electron microscopy measurements were performed on surface-adsorbed mucin samples from a bulk mucin concentration of 2 mg/ml that were deposited onto a hydrophobic carbon film (Figure 6) and a 1 mg/ml sample that was deposited onto plasma-treated hydrophilic carbon film (Figure 7). Analysis of these images gives $R_{TEM(hydrophobic)} = 6\pm2$ nm and $R_{TEM(hydrophilic)} = 7\pm1.5$ nm for the radius of the globular surface structures. Taking into account the shrinkage of the molecule during TEM sample

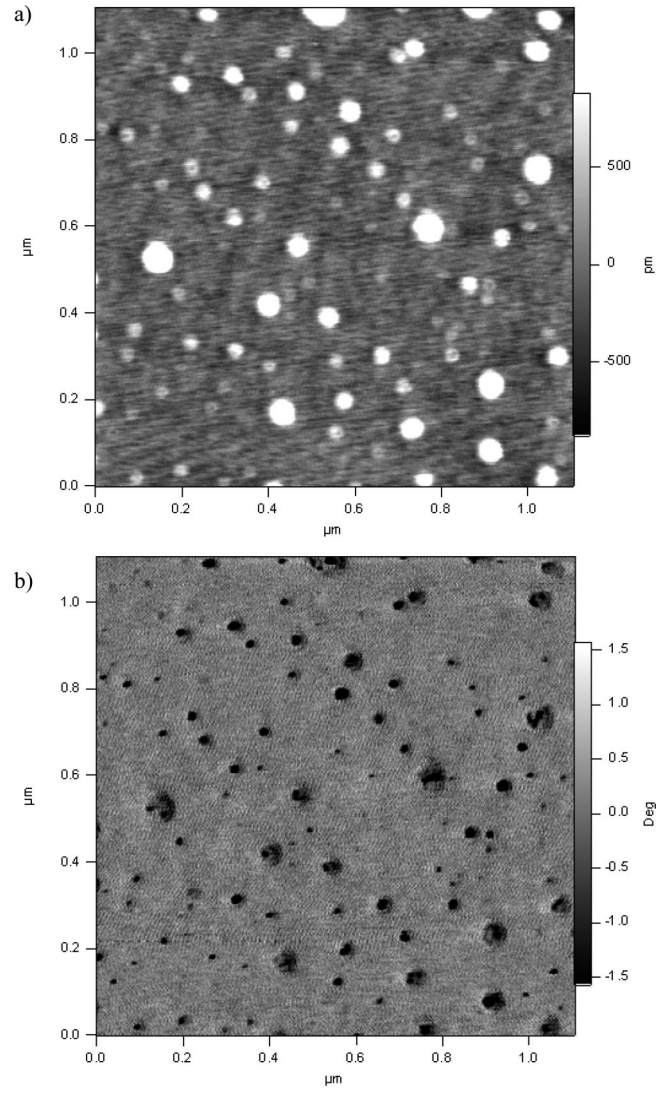

Figure 11. (a) AFM topography and (b) phase of mucin film deposited from sodium acetate buffer (pH = 4.9). The image was collected with a conventional AFM tip.

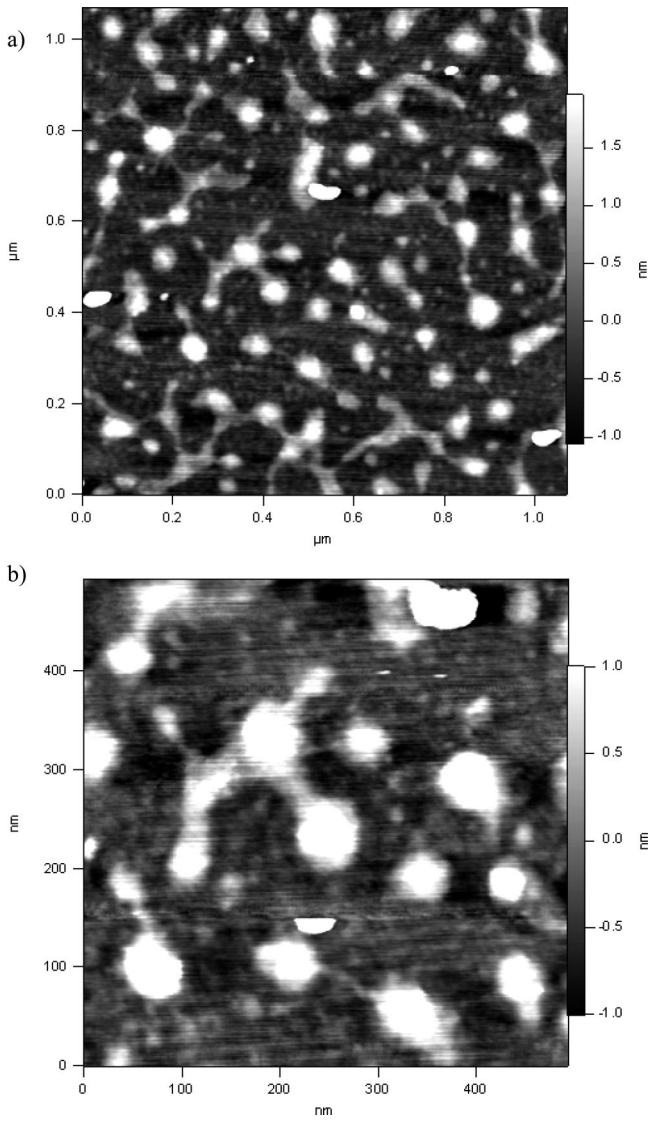

Figure 12. (a) AFM topography and (b) relative phase of mucin film deposited from sodium acetate buffer (pH = 4.9). The image was collected using a HI-RES tip.

preparation, these features are identified with daisy beads of the mucin molecule.

In Figures 8 and 9, AFM images are shown of mucin adsorbed from 30 mg/ml bulk solutions taken in air and in 10 mM NaCl solution, respectively. Features with radii bigger than those for the sample prepared from the very dilute mucin solution are observed, and the analysis provides values of $R_{AFM}^{dry} = 58\pm15$ nm and $R_{AFM}^{wet} = 107\pm21$ nm. These dimensions correspond to the size of the whole chain morphology.

Subsequent dilutions of the bulk solutions produce homogeneous coverage, and the analysis of images taken at 1, 0.1, and 0.01 mg/ml bulk concentrations is summarized in table 1. The structure of these adsorbed layers is found to be complex. In Figure 10, we present a high-resolution image of the layer formed from 1 mg/mL mucin solution. In the central area of the image, small domains can be observed similar to those visualized before (Figures 4) and identified as "daisy beads". If the first layer of mucin corresponds to the polyampholyte fence configuration, then subsequent layers are in the tail area of the Gouy–Chapman length and therefore adopt a pancake conformation.[67] In the case of the layer formed from 0.01 mg/ml solution, the radius of the adsorbed pancakes (~60 nm) can be

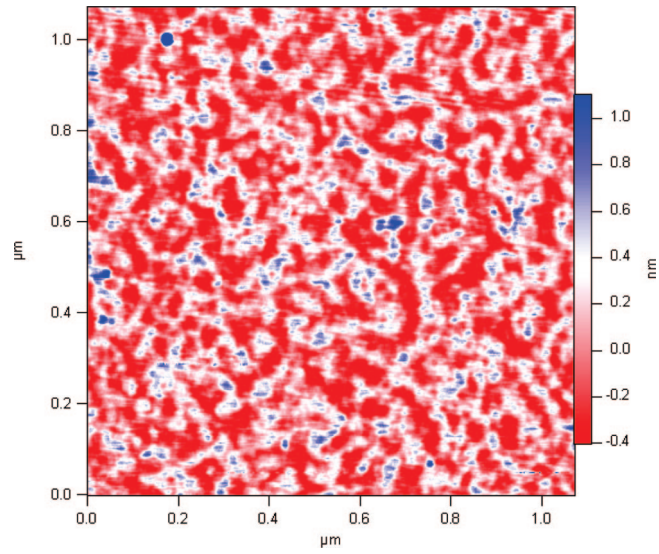

Figure 13. AFM topography of mucin film deposited from 1:1 water/ethanol mixture. The image was collected using a HI-RES tip.

correlated with the radius of gyration of a mucin molecule in bulk solution (R_g = 52 nm). There is no clear quantitative relationship between the radius of a pancake and the radius of gyration, but generally pancakes are wider than a three-dimensional coil or globule.

Because the observed globules have no internal structure, they can be analyzed as liquid drops, and the surface free energies of the globules to follow the Young−Laplace equation.[69] The contact angle can be easily calculated from the AFM images by assuming that globules can be represented as spherical caps, $\cos\theta = (R^2_{AFM} - h^2_{AFM})/(R^2_{AFM} + h^2_{AFM})$, where R_{AFM} and h_{AFM} are the radius and the height, respectively, derived from AFM images. The contact angle was found to be 10±3°, indicating that globules wet the surface with a strongly favorable surface/globule interaction. It was also inferred that the contact angle does not depend on the concentration of the bulk mucin within experimental error, and thus the process should be governed solely by the electrostatic interactions between mucin and the underlying substrate. For these contact angles, it is hard to distinguish between the "pancake" and spherical cup conformations because $h_{AFM}/R_{AFM} \ll 1$. Another interesting observation was made while comparing the effective volume of the cups ($V_{CAP} = 1/6\pi\cdot h_{AFM}\cdot(3R^2_{AFM} + h^2_{AFM})$) and volume of mucin molecule in the bulk $V_{BULK} = 4/3\pi\cdot R^3_G$. It appears that when adsorbed the mucin molecules occupy 3–7 times less volume then in the bulk, which potentially may indicate that upon adsorption, mucin indeed collapses in a dense configuration, with water being depleted. Such depletion would lead to a higher energy of adsorption per unit area in comparison with the case where only electrostatic mechanisms are involved.

In table 1, it is observed that both the average width of the mucin "pancakes" and the percentage surface coverage decreases with decreasing concentration of the bulk mucin. Another unusual property of the adsorbed mucin molecules is their tendency to associate; in Figure 10, most of the pancakes have a figure-eight shape, indicating two cojoined molecules.

Several methods of sample preparation were investigated, including $NiCl_2$ modification of the mica surface and deposition from acetate buffer and (1:1) water/ethanol mixtures. A 0.1 mg/ml mucin solution and a range of $NiCl_2$ solutions from 1 to 3 mM were used. The effect of the addition of $NiCl_2$ to the mica substrate did not lead to the unfolding of "Orthana" mucin

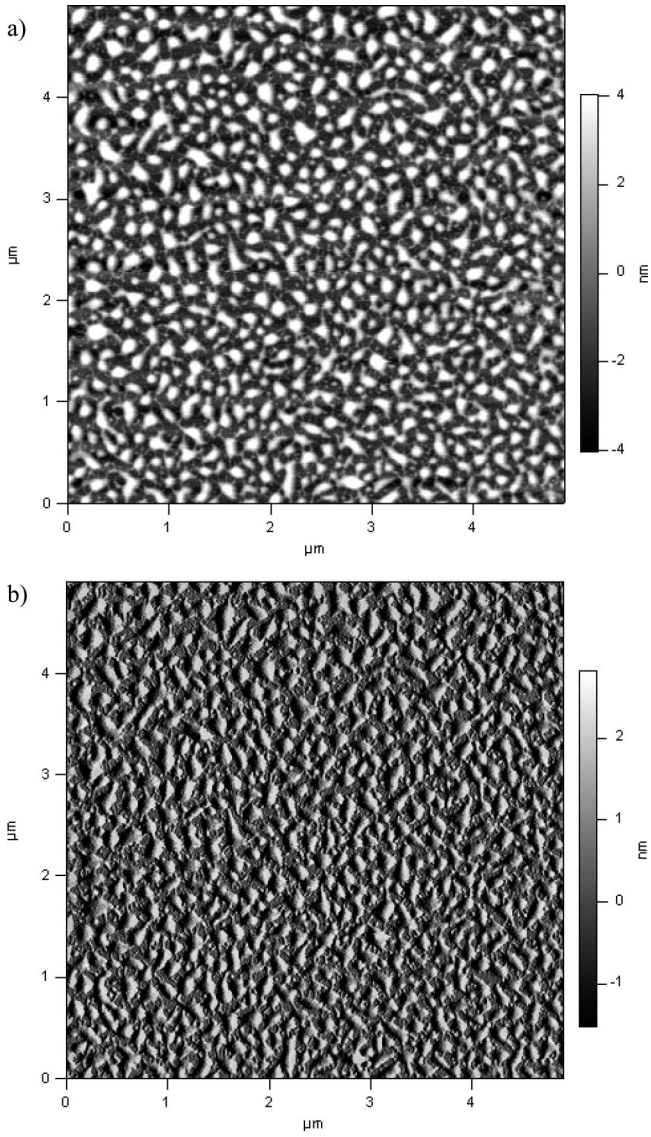

Figure 14. (a) AFM topography and (b) amplitude of mucin film deposited from pH 3 100 mM sodium acetate buffered mucin solution.

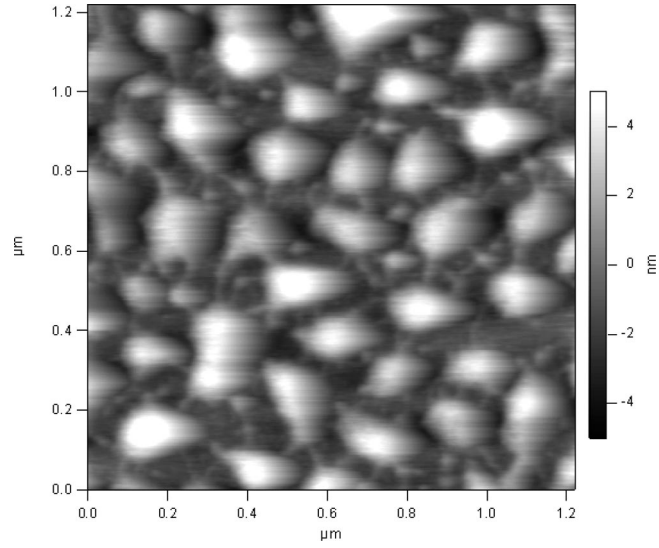

Figure 15. AFM topography of a mucin film deposited from pH3 100 mM sodium acetate buffer solution.

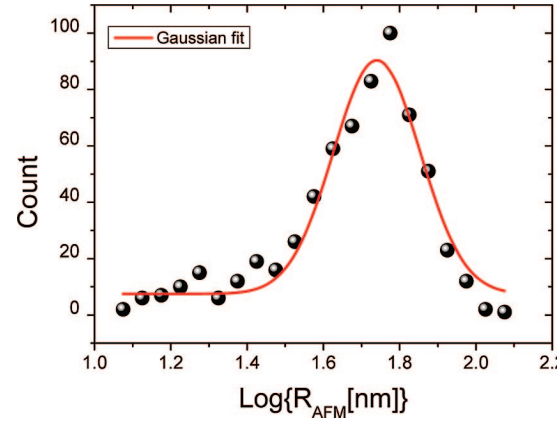

Figure 16. Size distribution histogram of mucin film deposited from pH 3 100 mM sodium acetate buffer solution.

molecules in contrast to the results of Brayshaw and McMaster for ocular mucin.[60]

The best results were achieved using water/ethanol mixtures and the acetate buffer. The crucial element was the use of HI-RES SPM probes (MikroMasch, Estonia) with extremely sharp diamond-like carbon extratips at the apex. The typical radius of curvature of an extratip is ~1 nm and its height is ~100–200 nm. Using a conventional SPM probe, images were obtained for mucins deposited from acetate buffer (40 mM, pH = 4.9, mucin concentration 0.1 mg/ml) (Figure 11) that are morphologically similar to those obtained using TEM (Figure 7). The image has two types of structures, namely "big" and "small". The phase image may indicate that "bigger" blobs consist of several smaller blobs. If we attribute these "small" features to daisy beads, then the possible number of beads per mucin molecule is ~2–4. Using HI-RES probes, links between the daisy beads could be visualized (Figure 12). A clearer representation of the chains is obtained for the molecules deposited from 1:1 water/ethanol mixtures (mucin concentration 0.01 mg/ml) (Figure 13). The naked chains are distinctively contrasted against the surrounding more compact daisy beads. The daisy chain model for the mucin molecule therefore finds strong evidence in both previous scattering experiments,[66] and the current ζ potential and imaging results. In addition the observed globular instability helps explain the liquid scaling of the structure factor peak ($c1/3$) of mucins measured in small-angle neutron-scattering experiments[39] above the chain overlap concentration (c^*). This is in contrast to the $c1/2$ scaling of the correlation length expected with linear polyelectrolytes. It is concluded that the mucin chains are in the "bead controlled regime" above c^*,[70,72] and it is the interbead distance that is measured in neutron experiments.

3.3. Effect of pH. Generally, pH has been shown to have a strong effect on mucin configurations.[2,8,51,52] Although nonsticky "Orthana" mucin does not exhibit a macrogel phase, in general, the aggregation of mucins is expected at both low and high values of pH.[2] One of the generic mechanisms observed is a cross-linking via hydrophobic domains that is especially relevant at low pH values, where negative charges are suppressed in the acidic environment.

To investigate the structure of mucin in an acidic environment, 100 mM sodium acetate buffer at pH 3 was used. The images of the adsorbed layer structures are presented in Figures 14 and 15. The average size of the domains is found to be 55±8 nm (Figure 16). These domains are most probably due to single mucin molecules interconnected through molecular bridges forming a gel-like or highly entangled structure at the sol

surface. The interconnecting chains, as well as daisy beads, can be seen from these images and suggest that some globular features may consist of daisy beads that belong to different mucin molecules.

4. Conclusions

The experimental investigation of "Orthana" mucin molecular conformation in aqueous solutions reveals a daisy chain configuration. The daisy beads are roughly spherical and are separated by flexible chains, presumably consisting of glycosylated fragments. The daisy beads are most likely due to intramolecular assemblies of hydrophobic domains that are surrounded by hydrophilic neighboring parts of the mucin molecule. The daisy chain conformation stems from both the polyampholyte and hydrophobic nature of the mucin, which has a relatively high proportion of basic amino acids and negatively charged sugars as well as the presence of hydrophobic domains. A single mucin molecule consisting of ~2–4 daisy beads interconnected via flexible chains, which is observed clearly in AFM and TEM images.

The value of ζ potential is found to be net negatively charged and relatively small in absolute value between −3 and −9 mV due to the absence of oligosaccharides with charged sialic acid residues. The mucin molecules act as weakly charged polyampholytes.

The adsorption of mucin onto hydrophilic surfaces is characterized by the formation of a complex morphology with different layer structures between the layers, namely fencelike structures and pancake-type structures that are probably formed by entangled aggregates trapped during adsorption.[53] The width of the mucin pancakes and their coverage decrease with decreasing concentration of the bulk mucin.

Acknowledgment. We all thank Ann-Marie Williamson for perpetual support of this project, Tony Weaver for the TEM measurements, Michael van Ginkel for immense help with the image analysis software, John Windust for crucial bioinformatics support on the mucin genetic types. G.Y. also thanks Tom McLeish, Jason Stokes, Damiano Rossetti, Bill Frith, Jeroen Bongaerts, Georgina Davies, and Asish Nandi for support and general discussions.

References and Notes

(1) Roussel, P.; Delmotte, P. *Curr. Org. Chem.* **2004**, *8* (5), 413–437.
(2) Bansil, R.; Turner, B. S. *Curr. Opin. Colloid Interface Sci.* **2006**, *11* (2–3), 164–170.
(3) Bansil, R.; Stanley, E.; Lamont, J. T. *Annu. Rev. Physiol.* **1995**, *57*, 635–657.
(4) Stokes, J. R.; Davies, G. *Biorheology* **2007**, *44* (3), 141–160.
(5) Wu, A. M.; Csako, G.; Herp, A. *Mol. Cell. Biochem.* **1994**, *137* (1), 39–55.
(6) Shi, L.; Caldwell, K. D. *J. Colloid Interface Sci.* **2000**, *224* (2), 372–381.
(7) Carlstedt, I.; Sheehan, J. K.; Corfield, A. P.; Gallagher, J. T. *Essays Biochem.* **1985**, *20*, 40–76.
(8) Cao, X. X.; Bansil, R.; Bhaskar, K. R.; Turner, B. S.; Lamont, J. T.; Niu, N.; Afdhal, N. H. *Biophys. J.* **1999**, *76* (3), 1250–1258.
(9) Blomberg, E.; Claesson, P. M. *Proteins Interfaces II* **1995**, *602*, 296–310.
(10) Bromberg, L. E.; Barr, D. P. *Biomacromolecules* **2000**, *1* (3), 325–334.
(11) Cassin, G.; Heinrich, E.; Spikes, H. A. *Tribol. Lett.* **2001**, *11* (2), 95–102.
(12) Berg, C. H.; Lindh, L.; Arnebrant, T. *Biofouling* **2004**, *20* (1), 65–70.
(13) Berg, I. C. H.; Rutland, M. W.; Arnebrant, T. *Biofouling* **2003**, *19* (6), 365–369.
(14) Lee, S.; Muller, M.; Rezwan, K.; Spencer, N. D. *Langmuir* **2005**, *21* (18), 8344–8353.
(15) Zappone, B.; Ruths, M.; Greene, G. W.; Jay, G. D.; Israelachvili, J. N. *Biophys. J.* **2007**, *92* (5), 1693–1708.
(16) Lindh, L.; Glantz, P. O.; Isberg, P. E.; Arnebrant, T. *Biofouling* **2001**, *17* (3), 227–239.
(17) Arvidsson, A.; Lofgren, C. D.; Christersson, C. E.; Glantz, P. O.; Wennerberg, A. *Biofouling* **2004**, *20* (3), 181–188.
(18) Hannig, M.; Herzog, S.; Willigeroth, S. F.; Zimehl, R. *Colloid Polym. Sci.* **2001**, *279* (5), 479–483.
(19) McMaster, T. J.; Berry, M.; Corfield, A. P.; Miles, M. J. *Biophys. J.* **1999**, *77* (1), 533–541.
(20) Berry, M.; McMaster, T. J.; Corfield, A. P.; Miles, M. J. *Biomacromolecules* **2001**, *2* (2), 498–503.
(21) Jay, G. D.; Harris, D. A.; Cha, C. J. *Glycoconjugate J.* **2001**, *18* (10), 807–815.
(22) Jay, G. D.; Haberstroh, K.; Cha, C. J. *J. Biomed. Mater. Res.* **1998**, *40* (3), 414–418.
(23) Jay, G. D.; Hong, B. S. *Connect. Tissue Res.* **1992**, *28* (1–2), 89–98.
(24) Malmsten, M.; Blomberg, E.; Claesson, P.; Carlstedt, I.; Ljusegren, I. *J. Colloid Interface Sci.* **1992**, *151* (2), 579–590.
(25) Glantz, P. O. J.; Arnebrant, T.; Nylander, T.; Baier, R. E. *Acta Odontol. Scand.* **1999**, *57* (5), 238–241.
(26) Shi, L. *Trends Glycosci. Glycotechnol.* **2000**, *12* (66), 229–239.
(27) Hannig, M.; Dobbert, A.; Stigler, R.; Muller, U.; Prokhorova, S. A. *J. Nanosci. Nanotechnol.* **2004**, *4* (5), 532–538.
(28) Proust, J. E.; Baszkin, A.; Boissonnade, M. M. *J. Colloid Interface Sci.* **1983**, *94* (2), 421–429.
(29) Berg, I. C. H.; Elofsson, U. M.; Joiner, A.; Malmsten, M.; Arnebrant, T. *Biofouling* **2001**, *17* (3), 173–187.
(30) Lori, J. A.; Nok, A. J. *Biomed. Mater. Eng.* **2004**, *14* (4), 557–563.
(31) Cleary, J.; Bromberg, L.; Magner, E. *Langmuir* **2004**, *20* (22), 9755–9762.
(32) Alexandridis, P.; Hatton, T. A. *Colloids Surf., A* **1995**, *96* (1–2), 1–46.
(33) Durrer, C.; Irache, J. M.; Duchene, D.; Ponchel, G. *J. Colloid Interface Sci.* **1995**, *170* (2), 555–561.
(34) Perez, E.; Proust, J. E. *J. Colloid Interface Sci.* **1987**, *118* (1), 182–191.
(35) Castillo, E. J.; Koenig, J. L.; , Anderson, J. M.; Jentoft, N. *Biomaterials* **1986**, *7* (1), 9–16.
(36) Lindh, L.; Glantz, P. O.; Carlstedt, I.; Wickstrom, C.; Arnebrant, T. *Colloids Surf., B* **2002**, *25* (2), 139–146.
(37) Papagiannopoulos, A.; Waigh, T. A.; Hardingham, T.; Heinrich, M. *Biomacromolecules* **2006**, *7* (7), 2162–2172.
(38) Vassilakos, N.; Rundegren, J.; Arnebrant, T.; Glantz, P. O. *Arch. Oral Biol.* **1992**, *37* (7), 549–557.
(39) Waigh, T. A.; Papagiannopoulos, A.; Voice, A.; Bansil, R.; Unwin, A. P.; Dewhurst, C. D.; Turner, B.; Afdhal, N. *Langmuir* **2002**, *18* (19), 7188–7195.
(40) Maheshwari, R.; Dhathathreyan, A. *J. Colloid Interface Sci.* **2006**, *293* (2), 263–269.
(41) Zhu, X.; DeGraaf, J.; Winnik, F. M.; Leckband, D. *Langmuir* **2004**, *20* (24), 10648–10656.
(42) Efremova, N. V.; Huang, Y.; Peppas, N. A.; Leckband, D. E. *Langmuir* **2002**, *18* (3), 836–845.
(43) Claesson, P. M.; Blomberg, E.; Froberg, J. C.; Nylander, T.; Arnebrant, T. *Adv. Colloid Interface Sci.* **1995**, *57*, 161–227.
(44) Proust, J. E.; Baszkin, A.; Perez, E.; Boissonnade, M. M. *Colloids Surf.* **1984**, *10* (AUG), 43–52.
(45) Perez, E.; Proust, J. E.; Baszkin, A.; Boissonnade, M. M. *Colloids Surf.* **1984**, *9* (4), 297–306.
(46) Zhu, Y. X.; Granick, S. *Macromolecules* **2003**, *36* (4), 973–976.
(47) Raviv, U.; Giasson, S.; Kampf, N.; Gohy, J. F.; Jerome, R.; Klein, J. *Nature* **2003**, *425* (6954), 163–165.
(48) Benz, M.; Chen, N. H.; Israelachvili, J. *J. Biomed. Mater. Res., Part A* **2004**, *71A* (1), 6–15.
(49) de Vicente, J.; Spikes, H. A.; Stokes, J. R. *J. Tribol.* **2006**, *128* (4), 795–800.
(50) Cardenas, M.; Elofsson, U.; Lindh, L. *Biomacromolecules* **2007**, *8* (4), 1149–1156.
(51) Hong, Z. N.; Chasan, B.; Bansil, R.; Turner, B. S.; Bhaskar, K. R.; Afdhal, N. H. *Biomacromolecules* **2005**, *6* (6), 3458–3466.
(52) Hong, Z.; Chasan, B.; Bansil, R.; Turner, B.; Bhaskar, K. R.; Afdhal, A. *Abstr. Pap. Am. Chem. Soc.* **2002**, *224*, U416–U416.
(53) McColl, J.; Yakubov, G. E.; Ramsden, J. J. *Langmuir* **2007**, *23*, 7096–7100.
(54) Deacon, M. P.; McGurk, S.; Roberts, C. J.; Williams, P. M.; Tendler, S. J. B.; Davies, M. C.; Davis, S. S.; Harding, S. E. *Biochem. J.* **2000**, *348*, 557–563.

CDV

(55) Harding, S. E.; Rowe, A. J.; Creeth, J. M. *Biochem. J.* **1983**, *209* (3), 893.
(56) Jumel, K.; Fogg, F. J. J.; Hutton, D. A.; Pearson, J. P.; Allen, A.; Harding, S. E. *Eur. Biophys. J. Biophys. Lett.* **1997**, *25* (5–6), 477–480.
(57) McMaster, T. *Clin. Chim. Acta* **2005**, *355*, S57–S58.
(58) Brayshaw, D. J.; Berry, M.; McMaster, T. J. *Ultramicroscopy* **2004**, *100* (3–4), 145–151.
(59) Round, A. N.; Berry, M.; McMaster, T. J.; Corfield, A. P.; Miles, M. J. *J. Struct. Biol.* **2004**, *145* (3), 246–253.
(60) Brayshaw, D. J.; Berry, M.; McMaster, T. J. *Ultramicroscopy* **2003**, *97* (1–4), 289–296.
(61) Round, A. N.; Berry, M.; McMaster, T. J.; Stoll, S.; Gowers, D.; Corfield, A. P.; Miles, M.J., *Biophys. J.* **2002**, *83* (3), 1661–1670.
(62) Berry, M.; McMaster, T. J.; Corfield, A. P.; Miles, M. J. *Invest. Ophthalmol. Visual Sci.* **1999**, *40* (4), S965–S965.
(63) Cardenas, M.; Lindh, L.; Rennie, A.; Amebrant, T. *Biophys. J.* **2007**, 38A–38A.
(64) Cardenas, M.; Arnebrant, T.; Rennie, A.; Fragneto, G.; Thomas, R. K.; Lindh, L. *Biomacromolecules* **2007**, *8* (1), 65–69.
(65) Raynal, B. D. E.; Hardingham, T. E.; Sheehan, J. K.; Thornton, D. J. *J. Biol. Chem.* **2003**, *278* (31), 28703–28710.
(66) Yakubov, G. E., Papagiannopoulos, A.; Rat, E.; Easton, R. L.; Waigh, T. A., *Biomacromolecules* **2007**, http://dx.doi.org/10.1021/bm700607w.
(67) Dobrynin, A. V.; Colby, R. H.; Rubinstein, M. *J. Polym. Sci., Part B: Polym. Phys.* **2004**, *42* (19), 3513–3538.
(68) Gunning, A. P.; Kirby, A. R.; Mackie, A. R.; Kroon, P.; Williamson, G.; Morris, V. J. *J. Microsc. Oxford* **2004**, *216*, 52–56.
(69) Johner, A.; Joanny, J. F. *J. Phys. II* **1991**, *1* (2), 181–194.
(70) Rubinstein, M.; Colby, R. H.; Dobrynin, A. V. *Phys. Rev. Lett.* **1994**, *73* (20), 2776–2779.
(71) Dobrynin, A. V.; Colby, R. H.; Rubinstein, M. *Macromolecules* **1995**, *28* (6), 1859–1871.
(72) Holterman, H. J.; Sgravenmade, E. J.; Waterman, H. A.; Mellema, J.; Blom, C. *J. Colloid Interface Sci.* **1989**, *128* (2), 523–532.

BM700721C